Redox-driven stable isotope fractionation in transition metals: Application to Zn electroplating

A. Kavner [a,*], S.G. John [b], S. Sass [c], E.A. Boyle [b]

[a] *Department of Earth and Space Sciences and Institute of Geophysics and Planetary Physics, University of California, Los Angeles, CA 90095, USA*
[b] *Department of Earth, Atmospheric and Planetary Sciences, Massachusetts Institute of Technology, Cambridge, MA 02139, USA*
[c] *Department of Chemical and Biomolecular Engineering, University of California, Los Angeles, CA 90095, USA*

Abstract

Redox processes are ubiquitous in Earth science and are often associated with large isotope fractionations. In a previous study, voltage-dependent amplification of stable isotope fractionation was observed for an Fe reduction process. Here, we describe experiments showing a similar effect for a second transition metal, zinc. After electrochemical reduction, the composition of plated Zn metal is enriched in the light isotope (^{64}Zn) with respect to the Zn^{2+} leftover in solution, with a voltage-dependent fractionation factor. Results from voltage-dependent electroplating experiments are in good agreement with a second data set following equilibrium fractional isotope evolution of Zn isotopes during an electroplating process which stepwise removes most of the Zn from the aqueous reservoir. Taken together, the results indicate a voltage-dependent isotope fractionation (in permil) of ^{66}Zn with respect to ^{64}Zn to be equal to −3.45 to 1.71 V. The negative slope trend is in contrast with previously published results on iron isotope fractionation during electroplating which shows a positive slope. These results are interpreted using an extension of Marcus theory, which predicts isotope fractionations as a function of driving force in an electrochemical system. Taken together with observations of natural fractionation of redox-sensitive and non redox-active elements, our modified Marcus theory provides a framework for quantitatively predicting transition metal isotope geochemical signatures during environmentally relevant redox processes in terms of simple energetic parameters.
© 2008 Elsevier Ltd. All rights reserved.

1. INTRODUCTION

Redox processes are among the fundamental geochemical processes of Earth and planetary evolution, with implications for the global cycling of all elements with multiple valence states—including carbon, oxygen, sulfur, and transition metals such as iron, chromium, and copper. As high resolution techniques for measuring transition metal isotope compositions have evolved over the past five to ten years, chemical isotope fractionations especially of Fe, have been observed in biological processes which take advantage of energy gained during electron charge transfer (redox) processes. Corresponding isotope fractionations associated with redox processes have been observed in both natural (often biological) and laboratory environments (e.g. Bullen et al., 2002; Ellis et al., 2002; Johnson et al., 2002; Roe et al., 2003; Anbar, 2004; Dauphas et al., 2004; Rouxel et al., 2005; Anbar and Rouxel, 2007). All naturally observed isotope signatures, whether biotic or abiotic in origin, must arise from the same physical laws of nature that also govern in the laboratory environment. A theory coupling stable isotope fractionation with electrochemical thermodynamics and kinetics is required to interpret geochemical signatures arising from redox processes operating in the natural world.

Much of the groundwork for understanding stable isotope fractionation in natural systems has been established for systems such as hydrogen, carbon, nitrogen, oxygen, and sulfur. Historically, fractionations have been classified according to the process causing isotopic separation

---

[*] Corresponding author. Fax: +1 310 825 2779.
E-mail address: akavner@ucla.edu (A. Kavner).

(Richter et al., 1998): An equilibrium fractionation arises from the differences in chemical activity of different isotope configurations expressed in terms of their partition functions (Urey, 1947; Bigeleisen and Mayer, 1947; Bigeleisen, 1955). A physical kinetic fractionation occurs due to differing rates of isotope transport processes within a phase (e.g. diffusion) or between phases (e.g. evaporation). Finally, a chemical kinetic isotope fractionation takes place when reaction rates differ for identical chemical species containing different isotopes. Each of these kinetic processes is characterized by its unique rate equation. A 2005 study examined voltage-dependent electrochemical fractionation associated with the electrodeposition of Fe (Kavner et al., 2005). This was the first study that showed an isotope fractionation that varied systematically as a function of kinetic driving force.

In this current paper, we continue our coupled theoretical and laboratory-based investigations of electrochemical isotope separation processes. We present the results of experiments designed to measure isotope fractionation during constant voltage electrodeposition of zinc metal in order to examine the redox-related isotope fractionation of Zn specifically, and transition elements in general. In order to interpret the new measurement, we appeal to a new fractionation factor arising from electrochemical processes, which combines previously distinct equilibrium and chemical kinetic fractionation factors. Zn was chosen for several reasons. First, it is an important stable isotope marker for anthropogenic contributions to Zn in the natural environment (John et al., 2007a). Although under normal circumstances Zn does not undergo redox changes in natural systems, Zn electrochemistry is important in several industrial processes. In addition, Zn charge transfer is easily controlled in the laboratory, using similar electrochemical experimental procedures which had been previously used to observe redox-related fractionations in Fe (Kavner et al., 2005). However, the Fe experiments were somewhat complicated by an inefficient electroplating process due to competition with the hydrogen evolution reaction. The Zn deposition kinetics are far more efficient than for Fe, allowing for better experimental control. Finally, Zn isotope separations can be measured with a precision better than 0.1‰, since Zn has been one of the transition element beneficiaries of the recent developments in the techniques of high resolution mass spectrometry (Marechal et al., 1999; Albaréde, 2004; Johnson et al., 2004; John et al., 2007a) and theoretical computational geochemistry (Schauble, 2003, 2004). Zn isotope electrochemistry provides a simple experimental framework within which to test our extension of Marcus theory to study redox kinetic isotope effects. This lays the groundwork for the application of Marcus–Kavner theory to environmentally relevant redox isotope effects.

2. EXPERIMENTAL PROCEDURE

2.1. Solution chemistry

We performed a series of experiments designed to measure isotope fractionation associated with electrochemical processes. All electroplating experiments were performed from an initial $ZnSO_4$ solution consisting of 1 M $ZnSO_4$ acidified in 1 M H_2SO_4. Using Web-PHREEQC, we determine that $Zn^{+2}[H_2O]_6$ is the predominant species in the starting solution, with $Zn(SO_4)$ species about an order of magnitude less abundant. All electrochemistry experiments were performed with respect to an Ag/AgCl standard electrode. The equilibrium potential was determined during a series of cyclic voltammetry experiments, and was found to be equal to $-1.02(\pm0.01)$ V with respect to the Ag/AgCl standard electrode. This is in good agreement with calculated standard reduction potentials of the Zn^{2+} deposition reaction. The counter electrode was a Pt electrode. All experiments were performed under regulated voltage (potentiostatic) conditions, and controlled so that a specific number of coulombs are allowed to pass during the course of an electroplating experiment.

Two separate sets of experiments were performed. The first set was designed to examine isotope fractionation as a function of kinetic driving force using a range of overpotentials varying from -25 mV to -800 mV, and a range of total coulombs passed, from 5 to 50 (Table 1). For each experiment, fresh 50 mL aliquots of starting solution and fresh 1 cm^2 glassy carbon electrodes were used. Prior to electroplating, the solution was de-oxygenated for 15–20 min using bubbled Ar. Bubbles were observed evolving from the cathode electrode surface during all experiments, presumably due to the competing hydrogen evolution reaction. Therefore, not all of the total coulombs passed during each experiment were efficient in generating Zn metal. We estimate plating efficiencies of approximately 50–90% for these experiments, much higher than the estimated 0.1–1% in the Fe experiments (Kavner et al., 2005). The total amount of material plated was varied in this series of experiments, but over a narrow range so that only very small amounts of Zn—0.5% or less—were plated in order to preserve a uniform reservoir stable isotope composition for this set of experiments.

Table 1
Design of experiments and summary of results of fractionation of electroplated Zn metal, reported in ‰ fractionation with respect to starting solution ($\delta^{66}Zn$)

| Overpotentials (in mV) | Charge (coulombs) | | | |
	5	10	20	50
25	−3.6 (±0.06)			
50		−3.39 (±0.04)		
100		−3.21 (±0.07)	−3.24 (±0.04)	−3.05 (±0.05)
			−3.31 (±0.06)	
200			−3.45 (±0.04)	−2.84 (±0.04)
800			−2.48 (±0.07)	

Reported errors are two-sigma standard errors from Zn isotope analysis in triplicate.

A second set of experiments was designed to follow mass balance and the Zn stable isotope evolution during a stepwise electroplating process designed to deplete the initial reservoir at a constant overpotential of −800 mV (Table 2). In these experiment, a single starting batch of plating solution was used, and a series of electroplating treatments (all at −800 mV) were performed. The cathode was removed approximately after each 1000 coulombs of reaction, and a fresh cathode was introduced to continue the experiment. The leftover plating solution was sampled twice towards the end of the experiment. The extent of reaction and the deposition efficiency was determined by measuring the mass of the electroplated Zn after each step.

After each electrodeposition step in both experiments, the cathode electrodes were removed from solution, gently rinsed in distilled water, weighed, and sent for mass spectrometry analysis. Zn isotope analysis was performed following the methods outlined in John et al. (2007a). Zn on the electrodes and in the $ZnSO_4$ plating solution was dissolved in 2% HNO_3 and diluted to a final concentration of 200 ppb Zn for isotopic analysis. Samples and standards were spiked with 100 ppb Cu in order to monitor instrumental mass bias. Samples were analyzed on an IsoProbe multi-collector ICP-MS (Thermo Scientific) equipped with an APEX-Q desolvating inlet system (ESI). Signal intensity was measured on masses 60, 63, 64, 65, 66, and 68. Data for each analysis was collected in eighteen 10-s blocks. All samples were analyzed in triplicate, interspersed with 200 ppb Zn standards prepared from NIST SRM 682. The relationship between Zn and Cu mass bias was determined empirically from the standards (Marechal et al., 1999), and this correction was applied to all samples. The ^{64}Zn signal on mass 64 was corrected for the presence of ^{64}Ni by monitoring the concentration of ^{60}Ni, though for these samples the correction was always insignificant. The addition of 50 μM H_2SO_4 to Zn standards did not change the measured isotope ratios, indicating the SO_4 from the electroplating bath would not interfere with our analyses. All isotope measurements are reported as permil deviations from the starting solution using a delta notation where:

$$\delta^{66}Zn = \left(\left((^{66}Zn/^{64}Zn)_{sample} / (^{66}Zn/^{64}Zn)_{Starting\ solution} \right) - 1 \right) 1000.$$

(1)

3. RESULTS

3.1. Isotope fractionation as a function of overpotential

The results from the fractionation vs. overpotential experiments (Fig. 1 and Table 1) show that electroplating creates a significant isotope separation of the electroplated zinc with respect to the starting solution, with light Zn pref-
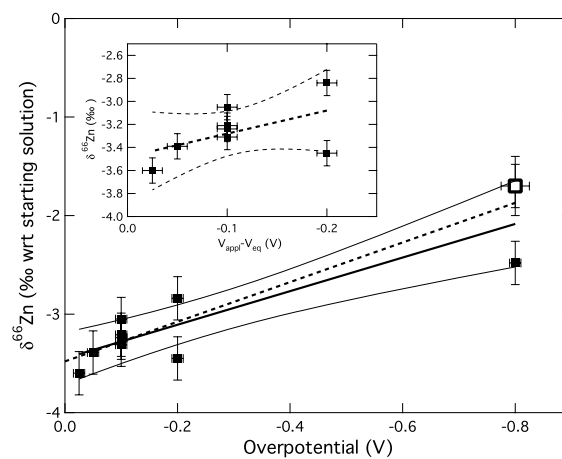

Fig. 1. Zn isotope fractionation as a function of overpotential with respect to the Zn^{II}/Zn metal equilibrium in the electroplating experiments shown in Table 1. The bold dashed line shows the weighted linear least squares fit through the data set only between −25 and −200 mV (inset, with two-sigma uncertainties). The best fit fractionation parameter obtained by modeling the isotope evolution data (cf. Fig. 3) is shown as an open square. The best fit weighted linear least square fit through the complete data set (including the two values at −800 mV) is shown as a bold line, with solid lines indicating 95% uncertainty bands.

Table 2
Evolution of isotope fractionation during electroplating experiments

Coulombs (cumulative)	Sample type	$\delta^{66}Zn$ (‰)	Zn collected (g, at each step)	% efficiency[b] (at each step)
Start solution	Solution	0.0(±0.06)	0.29	85.6
1000	Metal	−1.88(±0.03)	0.62	97.4
2000[a]	Metal		0.92	88.6
3000[a]	Metal		1.2	79.1
4045	Metal	−1.37(±0.09)	1.47	79.7
5045[a]	Metal		1.76	82.8
6080[a]	Metal		1.92	23.5
8088	Metal	−.57(±0.03)	0.29	
	Solution	1.32(±0.04)	Solution	51.9
10013	Metal	−0.23(±0.03)	2.1	85.6
	Solution	1.53(±0.04)	Solution	

All of the deposition experiments were performed at 800 mV overpotential. Error bars are two-sigma precision errors from Zn isotope analysis.
[a] Electrode was removed and the mass of electroplated Zn was measured; however no isotope analysis was performed.
[b] Efficiency = 100 × (grams collected × 2F)/(coulombs deposited in step × 65.36 g/mol).

erentially deposited (δ^{66}Zn = −3.5 to −2.45‰). These values are greater than the typical ∼0.5‰ range in isotope composition observed in a variety of common natural and anthropogenic sources on Zn (John et al., 2007a). In addition, the extent of isotope fractionation monotonically decreases as a function of increasing driving force. It is also apparent from the data in Fig. 1 and Table 1 that the observed experimental scatter about the fractionation vs. voltage trend is larger than the two-sigma error bars determined from the isotope analytical work.

The experimental design included a series of electrodeposition experiments as a function of coulombs passed, holding electrochemical potential constant (Fig. 2). Four repetitions of the −100 mV experiment were performed, at 10 coulombs, two at 20 coulombs, and one at 50 coulombs to test for reproducibility and any time-(non-voltage) dependent fractionation effects. The average value and standard deviation of these four measurements is equal to −3.20 ± 0.11‰. In addition, a trend emerges which shows a decreasing extent of fractionation as a function of coulombs passed equal to on average 0.0059‰ per coulomb. This corresponds to a total of 0.26‰ over the complete 45 coulomb experimental range of the experiments. The same sense of the trend is also evoked in the two data points at 200 mV overpotential and at 800 mV (Fig. 1); however there are indications that the coulomb-dependent trend increases with increasing voltage.

At a single potential, the number of coulombs passed is related to time via the relationship between coulombs, time and current: $\text{Coul} = \int i(t)dt$. If the current is constant throughout these experiments, then coulombs and time are equivalent variables. However, during the constant potential experiments, current decreases exponentially with time, and then approaches a steady state. This coulomb/time dependence may not be the only source of experimental scatter, and it is not yet experimentally clear what is the explanation behind the coulomb dependence. It is likely

that the experimental scatter, with its implicit coulomb/time dependence, arises because of the changing chemical environment directly adjacent to the electrode surface. The Zn electrodeposition is accompanied by hydrogen evolution, which may locally raise the pH at the electrode surface. This in turn may cause changes in the Zn speciation, which may affect the isotope fractionation and the electrodeposition kinetics. Other possible factors include temperature dependent fractionation effects, or isotope fractionation due to diffusion at an electrode. All of these are potentially important, and are likely interdependent, making a full understanding of the electrode behavior quite complicated. Diffusion-aided isotope separation will be discussed in the following section, and the more complicated issue of chemical behavior at the electrode (and its change with time) is currently under experimental and theoretical investigation. For now, we use the two-sigma deviation on the four 100 mV measurements as our best estimate of the individual errors on each fractionation measurement, instead of the two-sigma analytical errors, which are lower by factor of two.

A weighted least squares linear fit to the fractionation vs. voltage data between 25 and 200 mV (excluding the data at 800 mV overpotential) gives an electrochemical fractionation of δ^{66}Zn(‰) = −3.48(0.17)−2.01(1.33)V. These observed separation values correspond to fractionation factors $\alpha_{electroplating}$ equal to $(^{66}\text{Zn}/^{64}\text{Zn})_{plated}/(^{66}\text{Zn}/^{64}\text{Zn})_{plating solution}$ = 0.9965 at the equilibrium potential, and a prediction of a fractionation factor of 0.9981 at 800 mV. Our single measurement (in this data set) at 800 mV yields an electrochemical fractionation factor of 0.99752 (equal to −2.48‰), which is about 0.5‰ below the prediction of the data set up to 200 mV (but within the 98% confidence errors). As described in the next paragraph, the second set of experiments provides an additional, independent measurement of a fractionation factor at 800 mV. Together, the two measurements at 800 mV bracket the value predicted by the lower potential data set. In addition, the difference between the two data points mirrors the scatter in the data observed at 200 mV. Taken together, the weighted linear least squares fit through the complete data set yields an electrochemical fractionation δ^{66}Zn = −3.45(0.09)‰ to 1.71(0.24)*V‰. This fit through the full data set agrees exactly with the fit through the data set up to 200 mV. Therefore, we argue that the voltage dependence is a robust observation, despite the observed scatter in the data.

3.2. Mass balance and isotope evolution during the electrodeposition process

The second set of experiments was designed to evaluate mass balance and isotope evolution of plated metal and residual solution during depletion of Zn from the solution. During electroplating, the chemistry of the residual bath is evolving; hence, the equilibrium potential is evolving via the Nernst equation. Thus, the electrochemical driving force is evolving throughout the potentiostatic experiment. To analyze the electrochemical isotope evolution process, a simple numerical model was generated for the fractionation behav-
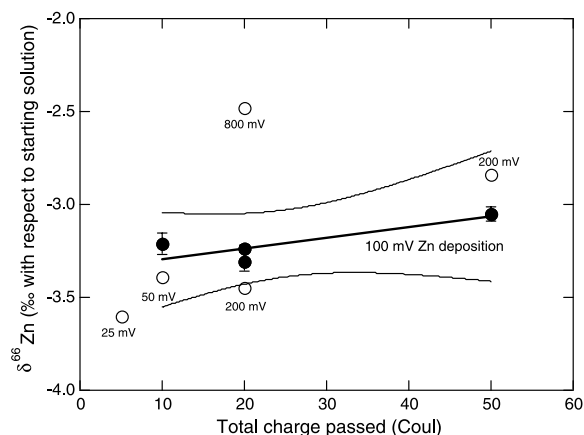

Fig. 2. Zn isotope fractionation as a function of total coulombs passed in the electroplating experiments. Solid black circles show the data at 100 mV. Moderate evolution with time is observed in this data set. Also shown is a weighted linear fit through the four points, and two-sigma error bars on the fit. The average and standard deviation of the four values is −3.20 ± 0.11‰. Two times the standard deviation is used as the error on each of the data points in Fig. 1.

ior in an electroplating system, assuming no diffusion-limited behavior at the electrode and perfect mixing within the solution (see Appendix A). Because of changes in solution behavior as the solution chemistry is modified during deposition of Zn at constant potential, the electroplating model is somewhat different than classical Rayleigh distillation, and current models provided by Ellis et al. (2002) and Dauphas and Rouxel (2006) for metal stable isotope separations. Since we observe a driving-force dependent isotope effect, this effect needs to be accounted for in the model for fractional isotope evolution during electroplating. The results of a simple, room temperature model are shown in Fig. 3. The best fit $\alpha_{electroplating}$ parameter, determined by the unweighted least squares fit to the four electroplated Zn and the two measurements of residual solution is equal $(^{66}Zn/^{64}Zn)_{plated}/(^{66}Zn/^{64}Zn)_{solution} = 0.9983$, corresponding to a permil fractionation equal to $-1.70‰$. Note that the observed fit is extremely sensitive to the estimate of the amount of starting solution, and the measurement of the amount of Zn plated in each step. For example, a 10% overestimate of the extent of reaction changes the best fit $\alpha_{electroplating}$ value so that it is equal to 0.9981, and in this case, the theoretical solid and solution isotope evolution lines fall through the complete data set with their error bars. Therefore, we interpret the best fit electrochemical fractionation factor and its error determined from the second set of experiments to be equal to $-1.7(\pm0.2)‰$. This error is consistent with the errors determined from analyzing the $-100 \, mV$ data (Fig. 2). Although more complicated models can be used, a model taking into account only the reservoir effect seems to explain the existing data set well.

Although our goal was to carry this experiment as close to completion as possible, we were limited by several factors. First, during the experiment, the temperature increased significantly, at about one degree/minute. We were concerned that this would affect the chemistry at the electrode and perhaps the fractionation as well. In addition,

as the experiment progressed, the Zn deposition became less and less efficient, requiring significantly more time at each step.

As shown by the linear extrapolation of the fractionation between 25 and 200 mV (dashed line in Fig. 1), the electrochemical fractionation factor determined from the independent isotope evolution experiments is in good agreement with the extrapolation of the low-coulomb experiments.

4. DISCUSSION

A weighted least-squares linear fit through all of the data, including the two values at 800 mV (bold line in Fig. 1) yields a voltage-dependent electrochemical isotope fractionation of Zn equal to $-3.45(\pm.009)‰$ to 1.71 $(\pm 0.24)‰$ V. The 95% uncertainty bands show that this result is statistically significant. Our first-order observation is that light isotopes of Zn are preferentially electroplated. This is consistent with a rule of thumb stating that higher oxidation states tend to favor heavier isotopes (Schauble, 2004).

The measured Zn isotope fractionation factors are significantly larger than those observed in most natural environments. Fractionations at a $\sim1‰$ level have been observed in a variety of natural samples including ferromanganese nodules, sediment trap material, marine carbonates, mosses, and cultured phytoplankton (Marechal et al., 1999; Pichat et al., 2003; Mason et al., 2005; Dolgopolova et al., 2006; Gelabert et al., 2006; John et al., 2007b). The largest naturally observed terrestrial isotope signatures for Zn are associated with hydrothermal systems, and span a range from $-0.43‰$ to $+1.33‰$ (Wilkinson et al., 2005; John et al., 2007c). Fractionations of up to 4‰ have been observed in iron meteorites (Luck et al., 2005). Fractionations on the order of $\sim-0.1‰$ to 1‰ are associated with a variety of laboratory experiments, including chromatog-
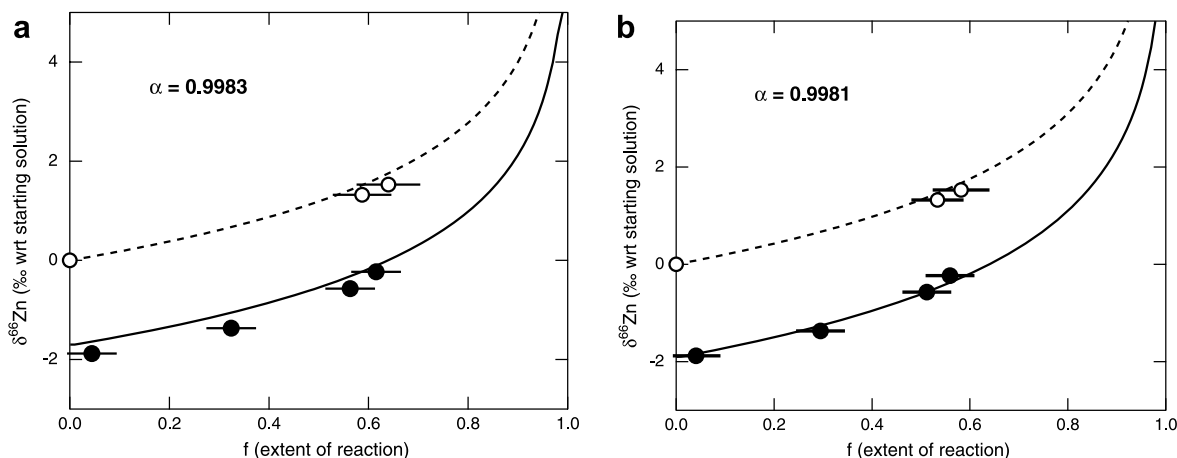

Fig. 3. Simple isotope evolution data and simple model of isotope fractionation during electroplating. Black lines show the weighted least squares best-fit model for evolution of electroplated zinc (solid) and remaining solution (dashed). Model assumes constant temperature, perfect mixing throughout the solution, and no time dependent and/or mass transport limited effects at the cathode electrode. (a) With data as given, best fit $\alpha_{electrochemical} = 0.9983$. (b) Assuming original data provides a 10% overestimate of fraction plated, the data yield a best fit $\alpha_{electrochemical} = 0.9981$, and a better fit through the data.

raphy (Ban et al., 2002; Marechal and Albarede, 2002) and centrifugation (Tcheltsov et al., 2006). Our results bolster the idea that redox processes are associated with a greater isotope fractionation than non-redox related chemical processes of the same element. It is significant that in the natural systems where observed fractionations are much lower than observed in the laboratory, Zn does not undergo redox processes, but remains as a 2^+ cation.

Similar redox-related amplification was observed for Fe isotope fractionations, where the largest observed fractionations were observed during electroplating (Kavner et al., 2005). Large isotope fractionations have also been observed during laboratory electrochemical reduction of other transition metals. For example, a 3.6‰ fractionation favoring light Cr in the reduced phase was observed during reduction of Cr in various aqueous environments (Ellis et al., 2002). The redox-related fractionation of Zn may help explain the large fractionations observed in iron meteorites (Luck et al., 2005). Correspondingly, fractionations observed due to non-redox related processes are mostly lower than 2‰ (e.g. Anbar, 2004).

Although redox-related isotope fractionations are observed in nature and in the laboratory, the only other system for which a voltage-dependent fractionation was explored was for the reduction of Fe^{2+} to Fe metal (Kavner et al., 2005). The magnitude of separation that was observed during Fe electroplating is similar to the fractionations observed during the same process for Zn, however, the Fe fractionation has an opposite voltage dependence. Although in both cases the lighter isotopes were preferentially deposited, in Fe the extent of fractionation increased with increasing driving potential, rather than decreased (Fig. 4).

A viable theory describing the nature of an electrochemical fractionation factor must predict isotope fractionation during electroplating, while also providing an explanation for the different voltage-dependent fractionation behavior of Zn and 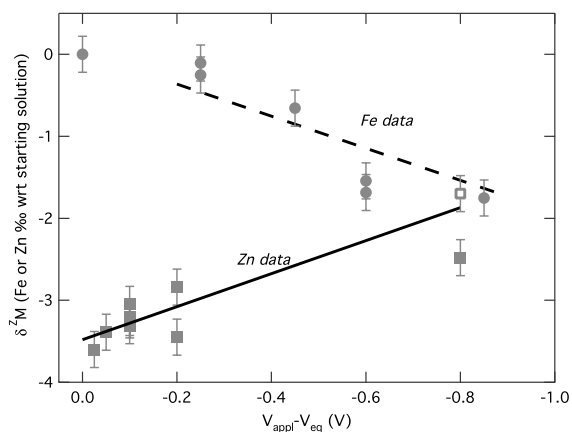Fe. Many distinct mechanisms contribute to the overall electroplating process, including mass transport to the electrode through the solution, several mechanistic steps involved in two electron transfers, phase change from aqueous ion to solid metal, aqueous speciation, and nucleation and growth of plated material on the electrode. Here we briefly consider two of these processes perhaps most likely to govern isotope fractionation in an electroplating environment, diffusive transport of species to the electrode surface, and the stable isotope dependent kinetics of an electron transfer reaction.

4.1. Diffusional mass transport

Although isotope separation by diffusion-limited transport to the electrode may contribute to the observed fractionation, several arguments bolster the idea that diffusion-limited mass transport cannot be solely responsible for our observed signature. In the first set of experiments, repeated plating experiments at the same overpotential (100 mV) yield the same overall fractionation, showing scatter on the level of ∼0.2‰ but no systematic time-dependence, which would be expected if the fractionation were diffusion limited. Also, hydrogen evolution which occurs at the electrode will likely provide significant convective mixing in any boundary layer. In addition, it is difficult to provide a consistent diffusion—limited mass transport model (Dauphas and Rouxel, 2006) that can have opposite fractionation vs. voltage effects in different systems, such as the Fe vs. Zn systems. Finally, recently published measurements of isotope separation during diffusion in Zn and Fe (Rodushkin et al., 2004) yield fractionation factors corresponding to ∼−0.16‰; much lower than those we observe in our experiments. Interestingly, our observed fractionations correspond to an estimate of the maximum isotope separation theoretically expected in a gaseous diffusion environment, predicted as $\left(\frac{1}{m_i} + \frac{1}{M}\right)^{-0.5}$, where M is the molecular mass of the gas through which the isotope of mass m_i is diffusing. For aqueous Zn^{2+}, however, the predicted fractionation due to difference in diffusion coefficients is equal to −3.33‰ for Zn (Rodushkin et al., 2004) because of the solution-coordination of Zn. In practice, even in gaseous diffusion processes, observed fractionations are significantly lower than theoretical values (Rodushkin et al., 2004). Therefore, if indeed diffusion-limited processes are responsible for the observed fractionation, then our understanding of fractionation during aqueous diffusion will likely need to be adjusted to account for the amplification of the effect during the electroplating process.

4.2. Isotope electrochemistry

In Kavner et al. (2005), electrochemical kinetic theory (Marcus, 1964, 1965) was expanded to include the behavior of an additional stable isotope system. A re-derivation of this theory is included in Appendix B. This theory predicts an electrochemical fractionation factor between isotopes l and k during a charge transfer reaction, following the equation given by:

Fig. 4. Linear trends in both Zn and Fe isotope fractionation in electroplating systems. Both are plotted on the same x and y-axis scale and as a function of voltage driving force, calculated with respect to Zn or Fe equilibrium standard reduction potential. The data are shown as gray symbols, and best fit lines through the data are shown with solid lines. Fe data is from Kavner et al., 2005.

$$\ln \alpha_{\text{electrochemical}}^{l-k} = \ln \left(\frac{k_0^l}{k_0^k} \right) + \frac{1}{2} \ln \alpha_{\text{eq}}^{l-k}$$

$$- \frac{(\Delta E_{\text{prod}}^{l-k} - \Delta E_{\text{react}}^{l-k})^2}{4\lambda kT}$$

$$+ \frac{\ln \alpha_{\text{eq}}^{l-k}}{2\lambda} ze(V_{\text{appl}} - V_{\text{eq}}), \qquad (2)$$

where l and k refer to two different stable isotopes of a single element; $\alpha_{\text{electrochemical}}$ is the electrochemical fractionation factor; the first term arises from the pre-exponential of the rate equation, and is a kinetic term related to the vibrational properties of the isotopes; $\alpha_{\text{equilibrium}}$ is the equilibrium fractionation factor between products and reactants; the term $\Delta E_{\text{prod}}^{l-k} - \Delta E_{\text{react}}^{l-k}$ relates the energy differences due to vibrational differences between the isotope systems in the product (metal) and reactant (aqueous) states, and is related to the equilibrium fractionation factor $\ln\alpha_{\text{eq}}$ (Bigeleisen and Mayer, 1947; Bigeleisen, 1955; Schauble, 2004). The term λ is a reorganization potential, describing the energetics of the vibrational state of the activation state of the reaction, and is derived in the work of Marcus (1964, 1965) (Marcus). z is the number of electrons transferred in the reaction (2 for Zn^{2+} to Zn_{metal}); e is the charge on an electron, k is Boltzmann's factor, and T is the temperature in Kelvin. It is important to note that this equation was derived for a single electron transfer in a homogeneous reaction; a much simpler system than our dual electron transfer and a phase change in our electroplating system.

This equation shows that isotope fractionation varies linearly with $V_{\text{appl}} - V_{\text{eq}}$, the electrochemical driving force (overpotential). The y-intercept is due to contributions from the first three terms, which arise from both kinetic (first term) and equilibrium (second and third terms) considerations. The slope of the relationship between fractionation and driving force is given by two terms: the λ reorganization energy which is always positive and on the order of $\sim 10^4$–10^5 J/mol, and the equilibrium fractionation factor $\ln(\alpha_{\text{equilibrium}})$, which is extremely sensitive to temperature, oxidation state, and speciation. Equilibrium fractionation factor can be either positive or negative; therefore Eq. (2) predicts that the slope of isotope fractionation vs. driving force can also be either positive or negative.

Deviations from linearity in the fractionation vs. voltage data are predicted in the presence of any anharmonicity of the activated state (i.e. a deviation from parabolic behavior along the reaction coordinate) may also yield curvatures on the fractionation vs. voltage behavior. This may explain an apparent curvature in both the Zn (concave down) and Fe (concave up) data; however in neither case can a curvature be determined in a statistically significant manner.

Eq. (2) predicts the voltage-dependent nature of our observed voltage-dependent isotope separation, and provides an elegant explanation for the different slopes of isotope separation vs. voltage in the Zn and Fe systems simply by invoking opposite signs of the equilibrium fractionation factor between isotopes l and k between products and reac-

tants ($1000 \ln \alpha_{\text{eq}}$) positive for $Fe_{\text{metal}}/[Fe^{+2}Cl_4]^{-2}$ and negative for $Zn_{\text{metal}}/Zn^{2+}$. The positive fractionation factor observed for the Fe system were in agreement with published theoretical predictions (Schauble et al., 2001). Since the voltage dependence of Zn fractionation has the opposite sense, this data for Zn makes a strong prediction that the equilibrium fractionation factor between Zn metal and Zn^{2+} in solution is negative. This result is in agreement with results for equilibrium Zn isotope fractionation presented by Schauble (2003).

5. CONCLUSIONS

Since redox processes are ubiquitous throughout the Earth, experimental electrochemical isotope geochemistry, with results interpreted by the modified Marcus theory, may provide a means to interrogate equilibrium fractionation factors and the energetics of solutions during reactions. The opposing sense of the electrochemical fractionation behavior for the two elements Zn and Fe (Fig. 3) confirms a specific prediction of the newly developed extension of the Marcus theory for electron transfer to encompass isotope behavior—namely that the fractionation vs. voltage plots may have either a positive or negative slope depending on the equilibrium isotope behavior of the chemical species being reduced. Neither a voltage dependence to an isotope fractionation nor a change in its slope can be accounted for using mass transport considerations. As far as we are aware, the modified Marcus theory is the only existing theory which provides a prediction for this observation. The only isotope-dependent term in Eq. (2) is the equilibrium fractionation factors between products and reactants, which can be either positive or negative, accounting for the negative and positive slopes. Electrochemical processes as described by the modified Marcus theory linearly amplify this equilibrium factor with an increase in the thermodynamic driving force for the reaction. The amplification constant is the reorganization energy, λ, which is sensitive to the liquid structure especially around the reacting species, and will likely be sensitive to changes in chemistry and speciation. Therefore, the modified Marcus theory combines redox (charge transfer) and speciation effects and also equilibrium and kinetic effects in a single process. This theory makes specific predictions of kinetic stable isotope fractionations in systems where redox processes may be occurring in the early solar system, on planets, and throughout the Earth, including in biological systems.

APPENDIX A. PROCEDURE FOR COMPUTING EVOLUTION OF ISOTOPES IN AN ELECTROPLATING SYSTEM

Function is written in IGOR (Wavemetrics) using IGOR macro language

```
Function Rayleigh_calcs(fraction, soln_a, soln_b, plated_a, plated_b, plated_delta, soln_delta, starting_moles, alpha)
wave soln_a, soln_b, plated_delta, soln_delta, plated_a, plated_b
wave fraction, alpha
variable starting_moles
variable f_counter
//this is a function to calculate isotope fractionation during electroplating to completion
//initial condition
//a is 66; b is 64
//we'll base this on soln_64 being nicely behaved, and calculate everything with respect to that
//these two establish the mass relationship for 64 zinc–this will set up the mass balance
soln_b = .5*starting_moles*(1 − fraction)
plated_b = .5*starting_moles-soln_b
//next, we have to deal with the initial condition
f_counter = 0
plated_delta[0] = alpha[0]
plated_a[0] = plated_b[0]*plated_delta[0]
soln_a[0] = starting_moles*.5-plated_a[0]
soln_delta[0] = soln_a[0]/soln_b[0]
//now we go on to the rest of the plating
f_counter = 1
do
   //new plated material is fractionated from previous concentration of solution
   plated_delta[f_counter] = alpha[f_counter]*soln_a[f_counter-1]/soln_b[f_counter-1]
   //mass balance determines the amount of Zn66
   //don't forget: only add on the stuff that we just plated!
   plated_a[f_counter] = plated_a[f_counter − 1] + (plated_b[f_counter]-plated_b[f_counter- 1])*plated_delta[f_counter]
   //mass balance determines the amount of Zn66 left in solution
   soln_a[f_counter] = starting_moles-soln_b[f_counter]- plated_a[f_counter]-plated_b[f_counter]
   soln_delta[f_counter] = soln_a[f_counter]/soln_b[f_counter]
   f_counter + = 1
while (f_counter < 100)
plated_delta = 1000*(1-plated_delta)
soln_delta = 1000*(1-soln_delta)
end
```

APPENDIX B. DERIVATION OF VOLTAGE-DEPENDENT ISOTOPE FRACTIONATION EQUATION

This section is adapted and extended from an earlier description in Kavner et al. (2005). Here, we provide a derivation of the isotope-dependent kinetics of the charge transfer reaction

$$ox + e^- \xrightarrow{k_{red}} red. \qquad (1)$$

We start with a picture, developed by Marcus, which represents the energy states of the reactants (ox) and producs (red) as two parabolas of energy as a function of reaction coordinate, ξ, with the same force constant, f, and a separation distance ξ, as shown in Fig. A1.

Eyring's rate equation for activated processes is:

$$k_{red} = k_{0,red} e^{\left(\frac{-E^*}{kT}\right)}, \qquad (2)$$

where E^* is the energy at the crossing point of the parabolas in Fig. A1, and is quadratic in terms of the thermodynamic (electrochemical) driving force of the reaction, $E_{driving\ force}$

$$E^* = \frac{f \xi_0^2}{4} + \frac{\Delta E_{drivingforce}}{2} + \frac{\Delta E_{drivingforce}^2}{4 f \xi_0^2}. \qquad (3)$$

The term $f \xi_0^2$ has the units of energy, is the single parameter describing the geometry of Fig. 1, and is known as the reorganization energy. In this derivation, $E_{driving\ force}$ is negative. Following the convention of writing $f \xi_0^2$ as a single "reorganization energy", λ we rewrite Eq. (3) as

$$E^* = \frac{\lambda}{4} + \frac{\Delta E_{drivingforce}}{2} + \frac{\Delta E_{drivingforce}^2}{4 \lambda}. \qquad (4)$$

The energy-reaction coordinate picture with a second isotope system is introduced in Fig. A2. The energy curves corresponding to the second (heavier) isotope system are offset due to differences in the zero point energies of the isotopologues: the molecules built with different
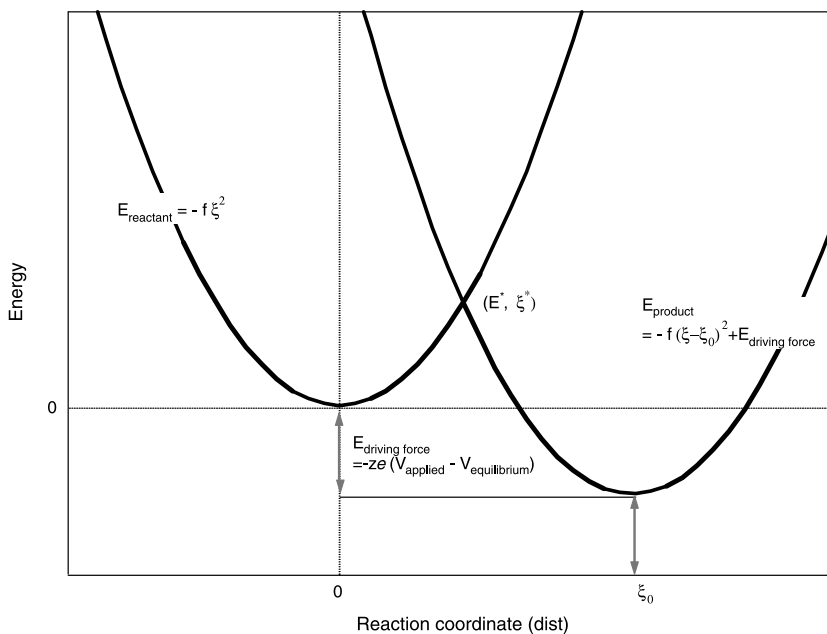
Fig. A1. Energy-reaction coordinate diagram for a homogeneous, single electron charge this reaction coordinate exists, and is equal to $f\xi_0^2$. The electrochemical driving force is equal to $-ze(V_{appl} - V_{eq})$.
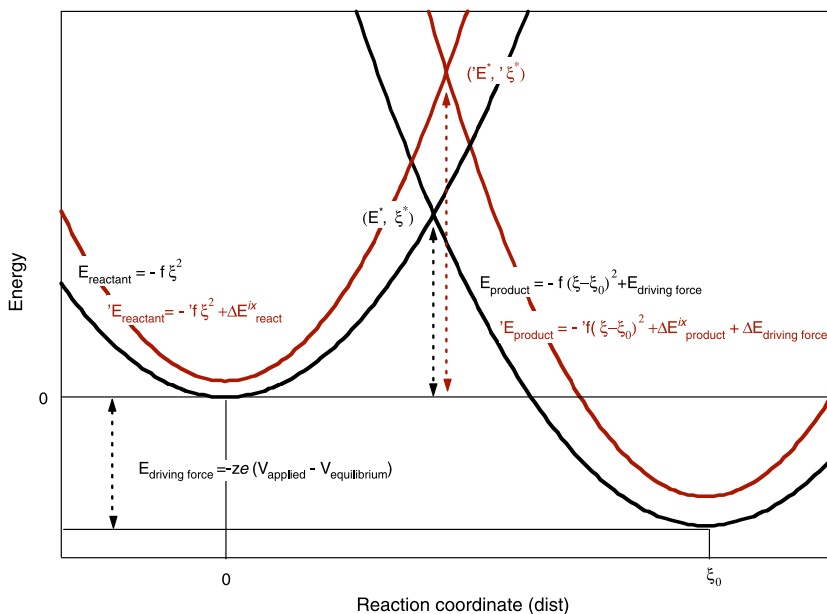

Fig. A2. Close-up of Marcus theory figure, with isotope effect included. Energy-reaction coordinate diagram, showing the behavior of a second isotopologue. The solid black curves correspond to reactants (left) and products (right) of chemical species. The gray curves correspond to a second (heavier) isotopologue of the same chemical species. The formulas for energies of all curves are written out explicitly in this Figure. The drawing is highly distorted: reorganization energies are in ~kiloJoules/mol while differences in energies between reactants and products are on the order of ~Joules/mol.

isotopes (e.g. Urey, 1947). As with the first isotope system, the energetics of the reactants and products of the second isotope system can be quantified by a single reorganization energy, λ'.[1] In this formulation, the reorganization energy is allowed to be different for the second isotope system.

The Eyring rate equation for the second isotopologue is

$$k'_{red} = k'_{0,red} e^{\left(\frac{-(E'^* - \Delta E'_{react})}{kT} \right)},$$ (5)

where the activation energy $E'^* - \Delta E'_{react}$ is equal to:

$$E'^* - \Delta E'_{\text{react}} = \frac{\lambda}{4} + \frac{1}{2}\Delta E_{df} + \frac{1}{2}(\Delta E'_{\text{prod}} - \Delta E'_{\text{react}})$$
$$+ \frac{((\Delta E'_{\text{prod}} - \Delta E'_{\text{react}}) + \Delta E_{df})^2}{4\lambda'}. \quad (6)$$

The difference in energies between the products and the reactants for the second isotope system with respect to the first, $\Delta E'_{\text{prod}} - \Delta E'_{\text{react}}$, is equal to $-k_b T \ln \alpha_{\text{eq}}$, where the term α_{eq} is the equilibrium isotope fractionation factor between products and reactants for the two isotope systems (Bigeleisen and Mayer, 1947; Urey, 1947).

The electrochemical isotope fractionation factor $\alpha_{\text{electrochemical}}$, describes the isotope partitioning arising from electrochemical processes and is related to the ratio of the rate constants for the two different isotopologues in the electron transfer reaction such that

$$\ln \alpha_{\text{electrochemical}} = \ln\left(\frac{k'}{k}\right)$$
$$= \ln\left(\frac{k'_0}{k_0}\right) + (E^* - (E^{*\prime}$$
$$- \Delta E'_{\text{react}})/(k_b T)), \quad (7)$$

where

$$E* - (E'^* - \Delta E'_{\text{react}}) = \frac{1}{4}(\lambda - \lambda') - \frac{1}{2}(\Delta E'_{\text{prod}} - \Delta E'_{\text{react}})$$
$$- \frac{(\Delta E'_{\text{prod}} - \Delta E'_{\text{react}})^2}{4\lambda'}$$
$$- \frac{(\Delta E'_{\text{prod}} - \Delta E'_{\text{react}})\Delta E_{df}}{2\lambda'}$$
$$+ \frac{\Delta E_{df}^2}{4}\left(\frac{1}{\lambda} - \frac{1}{\lambda'}\right). \quad (8)$$

Eqs. (7) and (8) predict an isotope fractionation due to electrochemical processes that has a quadratic dependence on the electrochemical driving force. The electrochemical isotope separation has contributions linear in driving force, quadratic in driving force, and constant, arising from four separate factors: the kinetic factor $\ln\left(\frac{k'_0}{k_0}\right)$, the equilibrium fractionation factor, $\Delta E'_{\text{prod}} - \Delta E'_{\text{react}} = -k_b T \ln \alpha_{\text{eq}}$, the value of the reorganization energy λ, and the difference between the reorganization energies of the isotopologues $(\lambda - \lambda')$.

Eq. (8) shows that if the reorganization energies are even slightly mass dependent, then voltage-dependent fractionation loses its linearity, and may show a curvature. This effect is sensitive to small deviations in reorganization energy, at a ppb level. In addition, any anharmonicity in the reorganization energies (i.e. deviations from parabolic behavior in Fig. A1) is also expected to generate nonlinearities in the voltage-dependent fractionation factors.

In this paper, as in Kavner et al. (2005), we assume a simplified form of Eq. (8) in which the reorganization energies of the isotopologues are equal. In that case, Eqs. (7) and (8) simplify to:

$$\ln \alpha_{\text{electrochemical}} = \ln\left(\frac{k'_0}{k_0}\right) + \frac{1}{2}\ln \alpha_{\text{eq}} - \frac{(\Delta E'_{\text{prod}} - \Delta E'_{\text{react}})^2}{4\lambda kT}$$
$$+ \frac{\ln \alpha_{\text{eq}}}{2\lambda}ze(V_{\text{appl}} - V_{\text{eq}}). \quad (9)$$

REFERENCES

Albarède F. (2004) The stable isotope geochemistry of copper and zinc. In *Geochemistry of Non-traditional Stable Isotopes*, vol. 55 (eds. C. M. Johnson, B. L. Beard and F. Albaréde), pp. 409–427. Reviews in Mineralogy. Mineralogical Society of America, Washington DC.

Anbar A. D. (2004) Iron stable isotopes: beyond biosignatures. *Earth Planet. Sci. Lett.* **217**, 223–236.

Anbar A. D. and Rouxel O. (2007) Metal stable isotopes in paleoceanography. *Ann. Rev. Earth Planet. Sci.* **35**, 717–746.

Ban Y., Nomura M. and Fujii Y. (2002) Isotope effects of zinc in crown ether chromatography. *J. Nucl. Sci. Tech.* **39**, 156–159.

Bigeleisen J. (1955) Statistical mechanics of isotopic systems with small quantum corrections. I. General considerations and the rule of the geometric mean. *J. Chem. Phys.* **23**, 2264–2267.

Bigeleisen J. and Mayer M. G. (1947) Calculation of equilibrium constants for isotopic exchange reactions. *J. Chem. Phys.* **15**, 261–267.

Bullen T., White A., Mandernack K. and Witte K. (2002) Iron isotope fractionation: does equilibrium or disequilibrium rule? *Geochim. Cosmochim. Acta* **66**, A110.

Dauphas N., Janney P. E., Mendybaev R. A., Wadhwa M., Richter F. M., Davis A. M., van Zuilen M., Hines R. and Foley C. N. (2004) Chromatographic separation and multicollection-ICPMS analysis of iron. Investigating mass-dependent and -independent isotope effects. *Anal. Chem.* **76**, 5855–5863.

Dauphas N. and Rouxel O. (2006) Mass spectrometry and natural variations of iron isotopes. *Mass Spectr. Rev.* **25**, 515–550.

Dolgopolova A., Weiss D. J., Seltmann R., Kober B., Mason T. F. D., Coles B. and Stanley C. J. (2006) Use of isotope ratios to assess sources of Pb and Zn dispersed in the environment during mining and ore processing within the Orlovka-Spokoi-noe mining site (Russia). *Appl. Geochem.* **21**, 563–579.

Ellis A. S., Johnson T. M. and Bullen T. D. (2002) Chromium isotopes and the fate of hexavalent chromium in the environment. *Science* **295**, 2060–2062.

Gelabert A., Pokrovsky O. S., Viers J., Schott J., Boudou A. and Feurtet-Mazel A. (2006) Interaction between zinc and freshwater and marine diatom species: surface complexation and Zn isotope fractionation. *Geochim. Cosmochim. Acta* **70**, 839–857.

John S. G., Park J. G., Zhang Z. and Boyle E. A. (2007a) The isotopic composition of some common forms of anthropogenic zinc. *Chem. Geol.* **245**, 61–69.

John S. G., Geis R. W., Saito M. A. and Boyle E. A. (2007b) Zinc isotope fractionation during high-affinity and low-affinity zinc transport by the marine diatom *Thalassiosira oceanica*. *Limnol. Oceanogr.* **52**, 2710–2714.

John S.G., Rouxel O.J., Craddock P.R., Engwall A.E. and Boyle E.A. (2007c). Zinc stable isotopes in seafloor hydrothermal vent fluids and chimneys. *EPSL*, in press, doi:10.1016/j.epsl.2007.12.011.

Johnson C. M., Beard B. L. and Albarede F. (2004) Overview and general concepts. In *Geochemistry of Non-traditional Stable Isotopes*, vol. 55 (eds. C. M. Johnson, B. L. Beard and F. Albaréde), pp. 1–24. Reviews in Mineralogy. Mineralogical Society of America, Washington DC.

Johnson C. M., Skulan J. L., Beard B. L., Sun H., Nealson K. H. and Braterman P. S. (2002) Isotopic fractionation between Fe(III) and Fe(II) in aqueous solutions. *Earth Planet. Sci. Lett.* **195**, 141–153.

Kavner A., Bonet F., Shahar A., Simon J. and Young E. (2005) The isotopic effects of electron transfer: an explanation for Fe isotope fractionation in nature. *Geochim. Cosmochim. Acta* **69**, 2971–2979.

Luck J. M., Ben Othman D. and Albarede F. (2005) Zn and Cu isotopic variations in chondrites and iron meteorites: early solar nebula reservoirs and parent-body processes. *Geochim. Cosmochim. Acta* **69**, 5351–5363.

Marcus R. (1964) Chemical and electrochemical electron-transfer theory. *Ann. Rev. Phys. Chem.* **15**, 155–196.

Marcus R. A. (1965) On the theory of electron-transfer reactions. VI. Unified treatment for homogeneous and electrode reactions. *J. Chem. Phys.* **43**, 679–701.

Marechal C. and Albarede F. (2002) Ion-exchange fractionation of copper and zinc isotopes. *Geochim. Cosmochim. Acta* **66**, 1499–1509.

Marechal C. N., Telouk P. and Albarede F. (1999) Precise analysis of copper and zinc isotopic compositions by plasma-source mass spectrometry. *Chem. Geo.* **156**, 251–273.

Mason T. F. D., Weiss D. J., Chapman J. B., Wilkinson J. J., Tessalina S. G., Spiro B., Horstwood M. S. A., Spratt J. and Coles B. J. (2005) Zn and Cu isotopic variability in the Alexandrinka volcanic-hosted massive sulphide (VHMS) ore deposit, Urals, Russia. *Chem. Geo.* **221**, 170–187.

Pichat S., Douchet C. and Albarède F. (2003) Zinc isotope variations in deep-sea carbonates from the eastern equatorial Pacific over the last 175 ka. *Earth Planet. Sci. Lett.* **210**, 167–178.

Richter F. M., Liang Y. and Minarik W. G. (1998) Multicomponent diffusion and convection in molten MgO–Al$_2$O$_3$–SiO$_2$. *Geochim. Cosmochim. Acta* **62**, 1985–1991.

Rodushkin I., Stenberg A., Andren H., Malinovsky D. and Baxter D. C. (2004) Isotopic fractionation during diffusion of transition metal ions in solution. *Anal. Chem.* **76**, 2148–2151.

Roe J. E., Anbar A. D. and Barling J. (2003) Nonbiological fractionation of Fe isotopes: evidence of an equilibrium isotope effect. *Chem. Geol.* **195**, 69–85.

Rouxel O. J., Bekker A. and Edwards K. J. (2005) Iron isotope constraints on the Archean and paleoproteozoic ocean redox state. *Science* **307**, 1088–1091.

Schauble E. A. (2003) Modeling zinc isotope fractionations. *Eos. Trans. Am. Geo. U* **84**, F232.

Schauble E. A. (2004) Applying stable isotope fractionation theory to new systems. In *Geochemistry of Non-traditional Stable Isotopes*, vol. 55 (eds. C. M. Johnson, B. L. Beard and F. Albaréde), pp. 65–111. Reviews in Mineralogy. Mineralogical Society of America, Washington DC.

Schauble E. A., Rossman G. R. and Taylor H. P. (2001) Theoretical estimates of equilibrium Fe-isotope fractionations from vibrational spectroscopy. *Geochim. Cosmochim. Acta* **65**, 2487–2497.

Tcheltsov A. N., Sosnin L. Y., Shipilov Y. D., Zaozersky Y. P., Khamylov V. K. and Pochekutova T. S. (2006) Centrifugal enrichment of zinc isotopes, their application in medicine and in increasing radiation safety in nuclear power plants. *Nucl. Instr. Methods Phys. Res. A* **561**, 52–57.

Urey H. C. (1947) The thermodynamic properties of isotopic substances. *J. Chem. Soc.*, 562–581.

Wilkinson J. J., Weiss D. J., Mason T. F. D. and Coles B. J. (2005) Zinc isotope variation in hydrothermal systems: preliminary evidence from the Irish Midlands ore field. *Econ. Geol.* **100**, 583–590.

Associate editor: Juske Horita